

CFRP shear strengthening of reinforced-concrete T-beams with corroded shear links

Qin, Shunde; Dirar, Samir; Yang, Jian; Chan, Andrew; Elshafie, Mohammed

DOI:

[10.1061/\(ASCE\)CC.1943-5614.0000548](https://doi.org/10.1061/(ASCE)CC.1943-5614.0000548)

Document Version

Peer reviewed version

Citation for published version (Harvard):

Qin, S, Dirar, S, Yang, J, Chan, A & Elshafie, M 2015, 'CFRP shear strengthening of reinforced-concrete T-beams with corroded shear links', *Journal of Composites for Construction*, vol. 19, no. 5, 04014081. [https://doi.org/10.1061/\(ASCE\)CC.1943-5614.0000548](https://doi.org/10.1061/(ASCE)CC.1943-5614.0000548)

[Link to publication on Research at Birmingham portal](#)

Publisher Rights Statement:

© 2014 American Society of Civil Engineers
Published as above

Eligibility for repository checked January 2015

General rights

Unless a licence is specified above, all rights (including copyright and moral rights) in this document are retained by the authors and/or the copyright holders. The express permission of the copyright holder must be obtained for any use of this material other than for purposes permitted by law.

- Users may freely distribute the URL that is used to identify this publication.
- Users may download and/or print one copy of the publication from the University of Birmingham research portal for the purpose of private study or non-commercial research.
- User may use extracts from the document in line with the concept of 'fair dealing' under the Copyright, Designs and Patents Act 1988 (?)
- Users may not further distribute the material nor use it for the purposes of commercial gain.

Where a licence is displayed above, please note the terms and conditions of the licence govern your use of this document.

When citing, please reference the published version.

Take down policy

While the University of Birmingham exercises care and attention in making items available there are rare occasions when an item has been uploaded in error or has been deemed to be commercially or otherwise sensitive.

If you believe that this is the case for this document, please contact UBIRA@lists.bham.ac.uk providing details and we will remove access to the work immediately and investigate.

1 **CFRP SHEAR STRENGTHENING OF REINFORCED CONCRETE T-**
2 **BEAMS WITH CORRODED SHEAR LINKS**

3
4 Shunde Qin¹; Samir Dirar²; Jian Yang³; Andrew H. C. Chan⁴; and Mohammed Elshafie⁵

6 **ABSTRACT**

7 This paper investigates the structural behavior of uncorroded as well as corroded RC T-
8 beams strengthened in shear with either externally bonded (EB) carbon fiber-reinforced
9 polymer (CFRP) sheets or embedded CFRP rods. Nine tests were carried out on RC T-beams
10 having an effective depth of 295 mm and a shear span to effective depth ratio of 3.05. The
11 investigated parameters are the shear link corrosion level (un-corroded, 7% corroded, or 12%
12 corroded) and type of CFRP strengthening system (EB CFRP sheets or embedded CFRP
13 rods). The unstrengthened beams with shear link corrosion levels of 7% and 12% had shear
14 strengths that were 11% and 14%, respectively, less than the shear strength of the un-
15 corroded unstrengthened beam. Both the embedded CFRP rods and EB CFRP sheets were
16 effective in enhancing the shear strength of tested beams but the effectiveness of both
17 strengthening systems decreased with increasing shear link corrosion level. The shear
18 strength enhancement provided by the embedded CFRP rods and EB CFRP sheets decreased
19 from 19% and 15%, respectively, to 12% and 11%, respectively, with the increase in shear
20 link corrosion level from 7% to 12%. Corrosion of the shear links did not have a significant

¹ Ph. D. Candidate, School of Civil Engineering, University of Birmingham, Edgbaston, Birmingham, B15 2TT, United Kingdom, E-mail: sxq482@bham.ac.uk

² Lecturer in Structural Engineering, School of Civil Engineering, University of Birmingham, Edgbaston, Birmingham, B15 2TT United Kingdom (corresponding author), E-mail: s.m.o.h.dirar@bham.ac.uk

³ Lecturer in Structural Engineering, School of Civil Engineering, University of Birmingham, Edgbaston, Birmingham, B15 2TT, United Kingdom, E-mail: j.yang.3@bham.ac.uk

⁴ Professor, School of Science, Information Technology and Engineering (Ballarat), Federation University Australia, Victoria 3350, Australia, E-mail: a.chan@federation.edu.au

⁵ Laing O'Rourke Lecturer in Construction Engineering, Department of Engineering, University of Cambridge, Cambridge, CB2 1PZ, United Kingdom, E-mail: me254@cam.ac.uk

21 effect on the beam stiffness. Premature debonding limited the effectiveness of the EB CFRP
22 sheets whereas the embedded CFRP rods did not exhibit signs of debonding and therefore
23 showed higher effectiveness.

24

25 **CE Database subject headings:** Beams; Corrosion; Epoxy; Fiber reinforced polymer;
26 Rehabilitation; Reinforced concrete; Rods; Shear strength; Sheets

27

28

INTRODUCTION

29 Annually, large amounts of money are spent on repairing corrosion-damaged reinforced
30 concrete (RC) structures. In the United Kingdom (UK) alone, it has been estimated that the
31 cost of repairing corrosion-damaged RC bridges is about £616.5 million (Broomfield, 2007).

32 In the United States, the situation is even worse as the annual estimated direct cost of
33 replacing or repairing corrosion-damaged bridges is \$8.3 billion (Koch et al., 2001). Other
34 countries in North America and Europe are faced with the same challenge, so emphasizing
35 the global significance of the issue.

36 The use of de-icing salts in cold regions and/or windborne salts in coastal/marine
37 environments are the main causes of chloride contamination of concrete (El-Maaddawy and
38 Chekfeh, 2013). Chlorides break down the protective passive layer of iron oxides around the
39 internal steel reinforcement and thereby facilitate the corrosion process. The volume of the
40 corrosion products, which is larger than that of the steel consumed in the corrosion process,
41 stresses the surrounding concrete and initiates cracking and spalling of the concrete cover (El
42 Maaddawy and Soudki, 2007).

43 Internal steel shear links are susceptible to corrosion due to their proximity to the outer
44 surfaces of concrete members. Corrosion of the internal steel shear links can have a
45 detrimental impact on the shear strength of RC beams, and may lead to sudden and

46 catastrophic brittle failure (Xia et al., 2011). There is thus scope for safe, practical, and
47 durable shear strengthening methods.

48 In the last two decades, the use of fiber-reinforced polymer (FRP) reinforcement for
49 retrofitting RC structures has become a field of much research interest. FRPs have several
50 advantages over classic strengthening techniques, such as design flexibility, ease of use, and
51 corrosion resistance. Methods for shear strengthening of RC beams using FRP composites
52 include externally bonded (EB) sheets (Dirar et al., 2012) or plates (Mofidi et al., 2014), near-
53 surface mounted (NSM) bars (Rahal and Rumaih, 2011), prestressed carbon fiber reinforced
54 polymer (CFRP) straps (Dirar et al., 2013) and embedded CFRP rods (Valerio et al. 2009;
55 Mofidi et al. 2012a). Compared with the EB and NSM shear strengthening methods, the deep
56 embedment (DE) technique – also known as the embedded through section technique –
57 (Valerio and Ibell 2003; Valerio et al. 2009; Mofidi et al. 2012a) offers better bond
58 performance between the concrete and the FRP reinforcement (Chaallal et al., 2011).

59 A careful review of the published literature reveals that research studies investigating the
60 shear behavior of RC beams strengthened using the DE technique is scarce. Moreover, very
61 few studies have considered the behavior of CFRP shear-strengthened RC T-beams with
62 corroded shear links (El-Maaddawy and Chekfeh, 2013). Furthermore, to date, there are no
63 research studies comparing the effectiveness of the EB and embedded CFRP shear
64 strengthening systems in the context of RC T-beams with corroded shear reinforcement.

65 This paper presents the results of nine tests on un-strengthened as well as CFRP-strengthened
66 RC T-beams with either un-corroded or corroded steel shear links. EB CFRP sheets or
67 embedded CFRP rods are used as shear strengthening systems in this study.

68

69

RESEARCH SIGNIFICANCE

70 The strength enhancement of corrosion-damaged concrete infrastructure is an application of
71 considerable economic importance, particularly in the case of bridges. This investigation
72 examines the effectiveness of two CFRP systems for shear strengthening of concrete
73 structures with corroded shear links. The effect of shear link corrosion level on the shear
74 force capacity and shear strength enhancement provided by the CFRP systems has been
75 elucidated. As a matter of interest to owners, managers, and designers of concrete
76 infrastructure, the investigated CFRP systems show potential for enhancing the shear strength
77 of corrosion-damaged concrete structures.

78

79

EXPERIMENTAL INVESTIGATION

80 The experimental program comprised 9 RC T-beams categorized into three groups as
81 summarized in Table 1. Each group included three beams with a targeted shear link corrosion
82 level in a given beam of 0% (i.e. un-corroded), 7%, or 15%. Different durations of exposure
83 to corrosion and applied current densities were used, as reported in Table 1, to corrode the
84 shear links. Further details about the accelerated corrosion process are given below.

85 Each beam had a two-part designation consisting of an alphabetical letter (N, R, or S)
86 followed by a number (00, 07, or 12). The alphabetical letter indicates that a beam was
87 unstrengthened (N), strengthened with embedded CFRP rods (R), or strengthened with EB
88 CFRP sheets (S). The number refers to the actual shear link corrosion level in a given beam.
89 Hence, the designation N00 refers to an unstrengthened un-corroded beam whereas the
90 designation R12 refers to a beam with an actual shear link corrosion level of 12% and
91 strengthened with embedded CFRP rods.

92 All beams were 2.7 m long and had T-shaped cross-sections (see Figure 1) in order to
93 simulate existing slab-on-beam RC structures. The web width (b_w), flange width, and flange

94 thickness were 125 mm, 260 mm, and 100 mm respectively. The beams had a shear span to
95 effective depth ratio of 3.05 and an effective depth (d) of 295 mm. The beams were designed
96 to fail in shear and had a significant difference between their unstrengthened shear force
97 capacity and their flexural capacity so as to provide a sufficient range over which the level of
98 shear strength enhancement could be measured.

99 All beams were reinforced with steel flexural and shear reinforcement. The longitudinal steel
100 reinforcement consisted of three 20 mm compression bars and four 25 mm tension bars. The
101 compression reinforcement was anchored with a 230 mm \times 50 mm \times 25 mm welded steel
102 plate at each end. The tension reinforcement was anchored with a 100 mm \times 100 mm \times 25
103 mm welded steel plate at each end so as to prevent bond failure. The internal steel shear links
104 were 8 mm in diameter. The spacing of the steel shear links was 275 mm centre-to-centre
105 within the test span and 100 mm centre-to-centre within the non-test span (see Figure 2a).
106 The steel shear link spacing of 275 mm ($0.93d$) is representative of earlier design practice in
107 the UK which allowed shear link spacing of up to the effective member depth (Concrete
108 Society, 2009).

109 The CFRP shear strengthening scheme consisted of either one layer of continuous U-shaped
110 EB CFRP sheets or 10 mm sand-coated embedded CFRP rods spaced at 275 mm centre-to-
111 centre. The CFRP rod spacing was chosen in such a way that the shear strength enhancement
112 provided by the DE bars would at least counteract the shear strength reduction due to the
113 higher shear link corrosion level. The bottom corners of the beams strengthened with the EB
114 CFRP sheets were rounded along the test span to avoid stress concentrations in the EB CFRP
115 reinforcement.

116 The beams were tested in a three-point bending configuration as shown in Figure 2. The
117 centreline of each support was 250 mm from the corresponding beam end. The centre-to-
118 centre distance between the support at the end of the test span and the hydraulic jack was 900

119 mm. Steel plates, 200 mm wide by 25 mm thick, were used as supporting plates whereas a
120 200 mm wide by 20 mm thick steel plate was used as a loading plate.

121

122 **Materials**

123 The beams were cast one at a time using the same concrete mixture proportions (cement:
124 water: aggregate: sand = 1: 0.65: 2: 3) and a maximum aggregate size of 10 mm. In order to
125 create a chloride concrete environment, 3% calcium chloride by mass of the cement was
126 added to the concrete mixtures used for casting the corroded beams.

127 The values of the cube compressive strength, cylinder split tensile strength, and flexural
128 strength, as obtained on testing day (i.e. either 28 days after casting for the un-corroded
129 beams or after the accelerated corrosion process for the corroded beams), are summarised in
130 Table 2. The targeted cube compressive strength (f_{cu}) was 30 MPa. However, due to
131 unintended quality control issues, there were differences between the targeted and actual cube
132 compressive strength values (see Table 2). In order to avoid such an unfortunate situation, it
133 is recommended that, where possible, all beams be cast at the same time using the same
134 concrete batch. This should at least ensure that all beams have comparable, if not similar,
135 concrete strength values.

136 Tensile tests were carried out on the steel reinforcement bars to quantify their mechanical
137 properties. The average test results for the strength and stiffness properties of the steel
138 reinforcement are summarised in Table 3. The average values reported in Table 3 were based
139 on three tested samples per bar. The standard deviation values for the strength and stiffness
140 properties of the steel reinforcement were negligible.

141 The CFRP sheets used to repair the T-beams were unidirectional woven carbon fiber fabrics.
142 They were used in conjunction with a two-component epoxy laminating resin to provide a
143 composite strengthening system. The thickness, tensile strength, ultimate strain, and elastic

144 modulus of the composite system as provided by the manufacturer are 1 mm, 986 MPa, 1%,
145 and 95.8 GPa respectively.

146 The 10 mm sand-coated CFRP rods had a tensile strength, elastic modulus, and ultimate
147 strain of 2172 MPa, 124 GPa, and 1.75% respectively. A commercially available high-
148 viscosity epoxy resin was used for anchoring the embedded rods. As specified by the
149 manufacturer, it had a bond strength, compressive strength, compressive modulus, tensile
150 strength, and elongation at failure of 12.4 MPa, 82.7 MPa, 1493 MPa, 43.5 MPa, and 2%
151 respectively.

152

153 **Accelerated corrosion process**

154 Figure 3 shows a schematic of the accelerated corrosion setup. Apart from the shear links
155 within a test span, the internal steel flexural and shear reinforcement in the corroded beams
156 together with the end plates were coated with aluminium pigmented epoxy to provide
157 corrosion protection.

158 After concrete casting and a 28-day curing period, a test span was encircled with a stainless
159 steel sheet and placed within a plastic tank containing 3% sodium chloride (NaCl) solution.

160 The NaCl solution level was maintained at just above the top surface of the stainless steel
161 sheet. The stainless steel sheet was connected to the cathode of a direct current (DC) power
162 supply unit. The shear links in the test span of R12 were connected to each other and then to
163 one of the positive terminals of the DC power supply unit. The shear links in the test spans of
164 the remaining beams were each connected to the positive terminals of the DC power supply
165 unit. The same DC power supply unit, which had twelve individually controllable positive
166 terminals, was used for all beams.

167 Three current density values; namely 140, 185, and 200 $\mu\text{A}/\text{cm}^2$; were used as detailed in
168 Table 1 to corrode the steel shear links. These current density levels, which are comparable

169 with the current density value of $160 \mu\text{A}/\text{cm}^2$ used by El-Maaddawy and Chekfeh (2013),
170 were based on the findings of El-Maaddawy and Soudki (2003) who indicated that a current
171 density higher than $200 \mu\text{A}/\text{cm}^2$ would result in exaggerated concrete strains and crack
172 widths.

173

174 **Corrosion level**

175 The targeted corrosion levels of 7% and 15% were chosen to represent medium and high
176 corrosion levels respectively. The 15% corrosion level was selected based on the findings of
177 Almusallam (2001) who showed that corrosion levels of about 12% resulted in significant
178 reductions in the yield and ultimate stresses and strains of steel reinforcing bars.

179 The theoretical time required to achieve such corrosion levels was calculated using Faraday's
180 law. The actual corrosion levels were determined after testing using gravimetric mass loss
181 analysis. Before casting the corroded beams, the original mass and length of the shear links to
182 be corroded were recorded. After testing, the corroded shear links were extracted from the
183 concrete and the recommendations of ASTM G1-03 (2011) were used to calculate the actual
184 corrosion level.

185

186 **Installation of CFRP sheets**

187 Before installing the CFRP sheets, the web of a test span was roughened with a grinder. The
188 rounded corners at the soffit (see Figure 1) were further smoothed to reduce stress
189 concentrations. The prepared surface was then cleaned with a wire brush and compressed air.

190 It was also ensured that the surface was dry and free from any oil or greasy substances.

191 Upon completion of the surface preparation process, the two-component epoxy resin was
192 used to impregnate the CFRP sheets. A uniform layer of epoxy was then applied to the web at
193 a thickness of approximately 1 mm. The epoxy was also used to fill any pores on the concrete

194 surface. A layer of the epoxy-impregnated CFRP sheets was then pressed gently onto the web.
195 A plastic trowel was used to remove air bubbles beneath the CFRP sheets. Eventually, a final
196 layer of epoxy was applied to protect the CFRP sheets. The composite material was then left
197 to cure at room temperature.

198

199 **Installation of CFRP rods**

200 In order to install the CFRP rods, 15 mm diameter vertical holes were created in the test
201 spans, through the centreline of the cross-section, at 138 mm, 413 mm, and 688 mm from the
202 centreline of the support. The vertical holes were created by installing 15 mm diameter
203 acrylic rods at the required positions within the steel reinforcement cage before casting the
204 concrete. The acrylic rods were removed from the concrete two days after casting. For Beams
205 R07 and R12, the vertical holes were blocked by rubber plugs before starting the accelerated
206 corrosion process.

207 Prior to installing the CFRP rods, the holes were cleaned by a wire brush and compressed air
208 to remove any cement or aggregate residues. The lower ends of the holes were sealed with
209 plastic sheets and a high viscosity epoxy adhesive was used to fill two third of the holes. The
210 CFRP rods were covered with a thin layer of the adhesive and inserted into the holes. Any
211 excess epoxy was removed. The plastic sheets at the lower ends of the holes were removed
212 two days after installing the CFRP rods.

213 It should be noted that Valerio et al. (2009) demonstrated that it was possible to install the
214 CFRP rods by drilling vertical holes upwards from the soffit. The procedure explained above
215 for installing the CFRP rods was used for simplicity as it did not require drilling holes.

216

217 **Instrumentation**

218 The load was applied at a displacement-controlled rate of approximately 0.1 mm/min
219 (equivalent to approximately 3 kN/min) using a 500 kN hydraulic jack. Loading was stopped
220 at each 15 kN up to approximately 85% of the estimated failure load in order to record crack
221 propagation.

222 A comprehensive and carefully planned measuring strategy was implemented. A 250 kN load
223 cell was placed under the support at the end of the test span to measure the actual shear force.
224 The vertical deflection under the applied load was measured using both linear resistance
225 displacement transducers (LRDTs) and dial gauges. Strain gauges (6 mm, 120 Ω) were
226 attached to the shear links in the test spans, CFRP sheets, and embedded CFRP rods as shown
227 in Figure 2.

228 The readings of the 250 kN load cell, LRDTs, and strain gauges were obtained using a data
229 logger. The readings of the dial gauges were manually recorded.

230

231

RESULTS AND DISCUSSION

232 Accelerated corrosion results

233 As can be seen in Table 4, the shear links in the test spans of N07, R07, S07, N12, R12, and
234 S12 had average actual corrosion levels of 6.4%, 7.6%, 6.0%, 12.2%, 12.3%, and 12.1%
235 respectively. Except for the shear links in the test span of R07, all the corroded shear links
236 had average actual corrosion levels that are less than the targeted corrosion levels of either
237 7% or 15%. The average differences between the targeted (based on Faraday's law) and
238 actual (based on gravimetric mass loss) corrosion levels were 11% and 23% for the shear
239 links with nominal corrosion levels of 7% and 15% respectively. Comparable results were
240 reported by Malumbela et al. (2012). El Maaddawy and Soudki (2003) suggested that, at
241 corrosion levels higher than 7%, the amount of corrosion products around the steel
242 reinforcement might hinder the diffusion of the Hydroxide and/or Ferrous ions through the

243 rust layer. This might explain the higher difference between the targeted and actual corrosion
244 levels for the shear links with a nominal corrosion level of 15%.

245 Table 4 shows that the current density values used in this study had insignificant effect on the
246 average actual corrosion levels. The shear links in the test spans of R12, N12, and S12 were
247 corroded using current density values of $140 \mu\text{A}/\text{cm}^2$, $185 \mu\text{A}/\text{cm}^2$, and $200 \mu\text{A}/\text{cm}^2$
248 respectively. However, the shear links in the three beams had approximately equal average
249 actual corrosion levels ranging from 12.1% to 12.3%.

250

251 **Shear strength**

252 Table 5 shows the total shear force attained by each beam at failure. As reported in Table 5,
253 the tested beams had variable cube compressive strengths and therefore it would be
254 inaccurate to directly compare their shear force capacities. In order to reasonably compare the
255 shear strength of the tested beams, the nominal shear stress at failure (V_{max}/b_wd) for each
256 beam was divided by the square root of its cube compressive strength, which is a measure of
257 concrete shear strength. The resulting values of normalized shear stress at failure
258 ($V_{max}/b_wd\sqrt{f_{cu}}$) were then divided by the corresponding value for N00 (i.e. 0.76) to calculate
259 the normalized shear stress at failure relative to N00 (see Table 5).

260 The effect of shear link corrosion level on the shear strength of the unstrengthened beams can
261 be inferred by comparing their normalized shear stresses at failure relative to N00. Increasing
262 the shear link corrosion level decreased the shear strength of N07 and N12 relative to that of
263 N00 by 11% and 14% respectively. As the corrosion level increases, the yield and ultimate
264 stresses and strains of the shear links decrease (Almusallam, 2001) and the bond performance
265 between the shear links and concrete deteriorates. This, in turn, reduces the steel contribution
266 to the shear force capacity which adversely affects the shear strength of the beams.

267 The shear link nominal corrosion level of 7% did not have a significant effect on the shear
268 strength of the strengthened beams. The difference between the normalized shear stresses at
269 failure for R00 and R07 was about 2%. Similarly, S00 and S07 had a difference of about 4%
270 between their normalized shear stresses at failure. At the actual corrosion level of 12%, the
271 strengthened beams (i.e. R12 and S12) had normalized shear stresses at failure that were
272 approximately 12% less than the corresponding values for the un-corroded beams (i.e. R00
273 and S00).

274 As can be seen in Table 5, all strengthened beams had higher normalized shear stresses at
275 failure than the corresponding unstrengthened beams. Of note is that R07 and R12 had
276 normalized shear stresses at failure that were 19% and 12% higher than the corresponding
277 values for N07 and N12 respectively whereas the corresponding percentage enhancements for
278 S07 and S12 were 15% and 11% respectively. The DE technique therefore seems more
279 effective than the EB technique in enhancing the shear strength of RC beams with corroded
280 shear links. The higher effectiveness provided by the DE technique may be explained by two
281 factors. First, the embedded CFRP rods are less susceptible to debonding issues due to the
282 better bond performance between the concrete core and the CFRP reinforcement (Chaallal et
283 al., 2011). Second, the CFRP rods can be embedded along the full effective depth of the beam
284 whereas the presence of the flange limits the effective depth of the EB CFRP sheets.

285 The effectiveness of both strengthening systems decreased with increasing shear link
286 corrosion level. At the lower shear link corrosion level, the strengthening systems enhanced
287 the normalized shear stresses at failure for R07 and S07 by 7% and 3% respectively relative
288 to that of N00 (i.e. the un-corroded unstrengthened beam). However, at the higher shear link
289 corrosion level, R12 and S12 had normalized shear stresses at failure that were 4% and 5%
290 lower respectively than the corresponding value for N00. Hence, the strengthening systems
291 were almost, but not quite, effective at returning R12 and S12 to their un-corroded shear

292 strength. The reduced effectiveness of the EB technique with increasing shear link corrosion
293 level may be explained by the reduced friction resistance at the shear link/concrete interface
294 which causes early separation of the lateral concrete cover after formation of inclined cracks
295 (El-Maaddawy and Chekfeh, 2013). Further research is required to identify the factors
296 affecting the reduced effectiveness of the DE technique with increasing shear link corrosion
297 level.

298

299 **Deflection response**

300 Figures 4a-4c show the shear force-deflection curves for the un-corroded, 7% corroded, and
301 12% corroded beams respectively. All beams featured a quasi-linear shear force-deflection
302 response up to peak shear force. The sudden drop in load at peak shear force is characteristic
303 of brittle (shear) failure. For each beam, the shear force at failure and the corresponding
304 deflection at the loading point are given in Table 5.

305 Except for the case of the un-corroded beams (Figure 4a), the unstrengthened and DE
306 strengthened beams had comparable stiffness at a given corrosion level whereas the EB
307 beams had a stiffer response. This trend is particularly evident in Figure 4b since N07, R07,
308 and S07 had comparable concrete strengths (see Table 5). Mofidi and Chaallal (2011)
309 suggested that some EB CFRP continuous sheets, although uniaxial, can still carry some load
310 in the direction perpendicular to the fiber orientation. This might explain the higher stiffness
311 of the EB beams compared with those of the unstrengthened and DE strengthened beams.

312 For the un-corroded beams, R00 had lower concrete strength compared with N00 and S00
313 (see Table 5). The relatively low concrete tensile strength of R00 (see Table 5) resulted in
314 flexural and shear crack formations at lower shear force values compared with N00 and S00.
315 Crack opening resulted in higher deflections at a given shear force and consequently lower
316 stiffness for R00.

317 Figure 4d presents the shear force-deflection curves for the beams strengthened with the EB
318 CFRP sheets. These beams had concrete cube compressive strengths ranging from 36.8 MPa
319 to 42.9 MPa. Figure 4d shows that corrosion level had insignificant effect on the deflection
320 response of the EB strengthened beams. Similar results confirming this finding were reported
321 by El-Maaddawy and Chekfeh (2013). Although not detailed in Figure 4 for brevity purposes,
322 the deflection response of both the unstrengthened and the DE strengthened beams was not
323 affected by corrosion level.

324

325 **Failure mode**

326 The failure modes of the unstrengthened beams are shown in Figure 5. All the unstrengthened
327 beams, regardless of the shear link corrosion level, exhibited a shear mode of failure due to
328 inclined cracks that ran from the support to the load point. In the web, the main inclined
329 cracks followed a path at an angle of approximately 32° , intersecting both the first (i.e. closer
330 to the support) and second (middle) shear links. The inclined cracks followed a much
331 shallower path (approximately 20°) in the flange, intersecting the third (inner) shear link just
332 below the top of the flange. Visual inspection of Beam N12 at failure (see Figure 5) revealed
333 that it had a wider main inclined crack compared with the corresponding cracks in Beams
334 N00 and N07. This was to be expected as the shear links with the 12.2% average corrosion
335 level offered less resistance to crack opening.

336 Figure 6 shows the failure modes of the beams strengthened with the DE technique. Similar
337 to the unstrengthened beams, R00, R07, and R12 failed in shear due to inclined cracks that
338 extended from the support to the load point. However, the inclined cracks in the beams with
339 embedded CFRP reinforcement were more distributed than the corresponding cracks in the
340 unstrengthened beams. It is well known that increasing the transverse reinforcement ratio in a
341 RC beam results in more distributed and narrower cracks (Zakaria et al., 2009). The crack

342 patterns of R00, R07, and R12 can therefore be attributed to the presence of the embedded
343 CFRP rods. Of note is that there was no sign of debonding between the embedded CFRP rods
344 and the surrounding concrete at failure.

345 Figure 7 shows the typical failure mode of the beams strengthened with the EB CFRP sheets.
346 Those beams failed due to inclined cracks that penetrated the flange and propagated towards
347 the load point. The crack propagation was accompanied by the debonding of the EB CFRP
348 sheets as depicted in Figure 7. The premature debonding of the EB CFRP sheets may be
349 prevented by anchoring the strengthening system to the concrete using compatible composite
350 anchors. This would increase the effectiveness of the EB CFRP sheets and consequently the
351 shear force carrying capacity of the beams (Eshwar et al. 2008; Mofidi et al. 2012b; Koutas
352 and Triantafillou 2013).

353

354 **Strain in the shear links and CFRP reinforcement**

355 This section reports on the strain in both the steel shear links and the CFRP strengthening
356 systems. Figure 2 shows the locations of the strain gauges attached to the steel and CFRP
357 shear reinforcement. For the purpose of interpreting results, the shear links and embedded
358 CFRP rods are categorized into outer, middle, and inner shear reinforcement (see Figure 2).
359 Similarly, the strain gauges attached to the EB CFRP sheets are categorized into outer,
360 middle, and inner gauges as depicted in Figure 2. Unfortunately, some strain gauges failed
361 during testing and hence their results were discarded.

362 Figure 8 shows the shear force-strain variations for the steel shear links. In general, the shear
363 links exhibited two stages of response during loading. In the first stage, the shear links were
364 inactive and therefore did not contribute to the shear force capacity. The second stage is
365 marked by the formation of inclined cracks at a shear force of approximately 50 kN to 75 kN.
366 This variation in inclined cracking shear force is attributable to the variation in concrete

367 tensile strength (see Table 2). After the formation of inclined cracks, the shear links
368 developed strain with increasing shear force until failure occurred.

369 The outer and middle shear links were more strained compared with the inner shear links.
370 This can be explained by the fact that the outer and middle shear links were intersected by the
371 main shear cracks. The inner shear links were located at a region which did not experience
372 much cracking.

373 At a given shear link location (i.e. outer, middle, or inner), a shear link in a beam
374 strengthened with the EB CFRP sheets (i.e. S00, S07, or S12) had less strain at a given shear
375 force than the corresponding shear link in a beam strengthened with the DE CFRP rods (i.e.
376 R00, R07, or R12). For example, between a shear force of 65 kN and 140 kN, the strain in the
377 middle shear link in S12 varied between 0.0001 and 0.0010 whereas the strain in the middle
378 shear link in R12 varied between 0.0003 and 0.0020. This result was influenced by two
379 factors. First, the EB CFRP sheets had higher axial rigidity per unit area (1533 MPa) than the
380 DE CFRP rods (283 MPa per rod). Second, the EB CFRP sheets were continuous whereas the
381 DE CFRP rods were located between the shear links (see Figure 2) and therefore could not
382 reduce the strain in the shear links in a similar way to the EB CFRP sheets.

383 Figure 9(a) shows the shear force-strain variations for the embedded CFRP reinforcement.
384 The behaviour of the embedded CFRP rods was comparable to that of the steel shear links.
385 The shear forces at which the embedded rods started to function were also in the range of 50
386 kN to 75 kN. For Beam R12, the middle CFRP rod experienced the highest strain at a given
387 shear force as it was intersected by the main shear crack (see Figure 6). At peak shear force,
388 the strain in the embedded CFRP rods was in the range of 0.0013 to 0.0033.

389 The shear force-strain curves for the EB CFRP sheets are shown in Figure 9(b). The response
390 of the CFRP sheets can be divided into three phases. Initially, the sheets were inactive up to a
391 shear force of approximately 50 kN to 75 kN. At that shear force level, which marks the

392 beginning of the second phase, the sheets started to develop tensile strain as they started to
393 resist crack opening. For a given beam, the regions of the CFRP sheets intersected by the
394 inclined cracks developed strain at a higher rate than the remaining regions of the
395 strengthening system. In the third phase, the fabrics started to debond, as shown by the
396 reversing of the shear force-strain curves in Figure 9(b), and finally peeled off. At peak shear
397 force, debonding limited the highest recorded strain in the CFRP sheets to 0.0013.

398

399

CONCLUSIONS

400 This paper presents the results of an experimental investigation on the structural behavior of
401 un-strengthened as well as CFRP-strengthened RC T-beams with either un-corroded or
402 corroded steel shear links. The tested beams were strengthened with either EB CFRP sheets
403 or embedded CFRP rods. The actual shear link corrosion levels, obtained using gravimetric
404 mass loss, were 0% (un-corroded), 7%, and 12%. Based on the results of this study, the
405 following conclusions are drawn:

- 406 1. The unstrengthened beams with shear link corrosion levels of 7% and 12% had shear
407 strengths that were 11% and 14% respectively less than the shear strength of the un-
408 corroded unstrengthened beam.
- 409 2. The shear link corrosion level of 7% did not have a significant effect on the shear
410 strength of the strengthened beams. The beams with the shear link corrosion level of
411 7% and strengthened with the DE or EB CFRP systems had comparable shear
412 strengths to the corresponding un-corroded strengthened beams.
- 413 3. At the shear link corrosion level of 12%, the strengthened beams had shear strengths
414 that were approximately 12% less than the corresponding values for the un-corroded
415 strengthened beams. Moreover, the strengthened beams had shear strengths that were
416 approximately 4% to 5% less than the shear strength of the un-corroded

417 unstrengthened beam. Hence, the strengthening systems were almost, but not quite,
418 effective at returning the beams with the 12% shear link corrosion level to their un-
419 corroded shear strength.

420 4. The effectiveness of both strengthening systems decreased with increasing shear link
421 corrosion level. The shear strength enhancement provided by the DE and EB CFRP
422 systems decreased from 19% and 15% respectively to 12% and 11% respectively with
423 the increase in shear link corrosion level from 7% to 12%.

424 5. The corrosion level had insignificant effect on the deflection response of the tested
425 beams.

426 6. The beams strengthened with the EB technique had stiffer response and less strain in
427 the shear links compared with the corresponding beams strengthened with the DE
428 technique.

429 7. Debonding resulted in limited strain in the CFRP sheets (less than 0.0013). On the
430 other hand, the embedded CFRP rods did not show signs of debonding and developed
431 higher strains (0.0013 – 0.0043) compared with the EB sheets.

432

433

ACKNOWLEDGEMENTS

434 The authors would like to thank Fyfe Europe for supplying the CFRP sheets and epoxy
435 laminating resin used in this study. The first author acknowledges the financial support of the
436 UK Engineering and Physical Sciences Research Council.

437

438

REFERENCES

439

440 Almusallam, A.A. (2001). "Effect of degree of corrosion on the properties of reinforcing steel
441 bars." *Constr. Built. Mater.* 15 (8), 361-368.

442

443 ASTM International. (2011). "Standard practice for preparing, cleaning, and evaluating
444 corrosion test specimens." *ASTM G1-03*, West Conshohocken, PA.

445

446 Broomfield, J. P. (2007). "Corrosion of Steel in Concrete: Understanding, Investigation and
447 Repair." 2nd Edition, Taylor and Francis Group, Oxford, United Kingdom.

448

449 Chaallal, O., Mofidi, A., Benmokrane, B., and Neale, K. (2011). "Embedded through-section
450 FRP rod method for shear strengthening of RC Beams: performance and comparison with
451 existing techniques." *J. Compos. Constr.*, 15(3), 374-383.

452

453 Concrete Society. (2009). "Historical approaches to the design of concrete buildings and
454 structures." *Tech. Rep. No. 70*, Crowthorne, United Kingdom.

455

456 Dirar, S., Lees, J., and Morley, C. (2012). "Precracked reinforced concrete T-beams repaired
457 in shear with bonded carbon fiber-reinforced polymer sheets." *ACI Struct. J.*, 109(2), 215-224.

458

459 Dirar, S., Lees, J. M., and Morley, C. T. (2013). "Precracked reinforced concrete T-beams
460 repaired in shear with prestressed carbon-fiber reinforced polymer straps." *ACI Struct. J.*,
461 110(5), 855-866.

462

463 El-Maaddawy, T., and Chekfeh, Y. (2013). "Shear strengthening of T-Beams with corroded
464 stirrups using composites." *ACI Struct. J.*, 110(5), 779-790.

465

466 El Maaddawy, T., and Soudki, K. (2007). "A model for prediction of time from corrosion
467 initiation to corrosion cracking." *Cement Concrete Comp.*, 29, 168-175.

468

469 El-Maaddawy, T. A., and Soudki, K. A. (2003). "Effectiveness of impressed current
470 technique to simulate corrosion of steel reinforcement in concrete." *J. Mater. Civ. Eng.*, 15
471 (1), 41-47.

472

473 Eshwar, N., Nanni, A., and Ibell, T. J. (2008). "Performance of two anchor systems of
474 externally bonded fiber-reinforced polymer laminates." *ACI Mater. J.*, 105(1), 72-80.

475

476 Koch, G. H., Brongers, M. P. H., Thompson, N. G., Virmani, Y. P., and Payer, J. H. (2001).
477 "Corrosion cost and preventive strategies in the United States." Report No. FHWA-RD-01-
478 156, Federal Highway Administration, U.S. Department of Transportation, McLean, VA,
479 82pp.

480

481 Koutas, L., and Triantafillou, T. C. (2013). "Use of anchors in shear strengthening of
482 reinforced concrete T-beams with FRP." *J. Compos. Constr.*, 17(1), 101-107.

483

484 Malumbela, G., Moyo, P., and Alexander, M. (2012). "A step towards standardising
485 accelerated corrosion tests on laboratory reinforced concrete specimens." *J. S. Afr. Inst. Civ.
486 Eng.*, 54(2), 78-85.

487

488 Mofidi, A., and Chaallal, O. (2011). "Shear strengthening of RC beams with externally
489 bonded FRP composites: Effect of strip-width-to-strip-spacing ratio." *J. Compos. Constr.*,
490 15(5), 732-742.

491

492 Mofidi, A., Chaallal, O., Benmokrane, B., and Neale, K. (2012a). "Experimental tests and
493 design model for RC beams strengthened in shear using the embedded through-section FRP
494 method." *J. Compos. Constr.*, 16(5), 540-550.

495

496 Mofidi, A., Chaallal, O., Benmokrane, B., and Neale, K. (2012b). "Performance of end-
497 anchorage systems for RC beams strengthened in shear with epoxy-bonded FRP." *J. Compos.*
498 *Constr.*, 16(3), 322-331.

499

500 Mofidi, A., Thivierge, S., Chaallal, O., and Shao, Y. (2014). "Behavior of reinforced concrete
501 beams strengthened in shear using L-shaped CFRP plates: experimental investigation." *J.*
502 *Compos. Constr.*, 10.1061/(ASCE)CC.1943-5614.0000398, 04013033.

503

504 Rahal, K. N., and Rumaih, H. A. (2011). "Tests on reinforced concrete beams strengthened in
505 shear using near surface mounted CFRP and steel bars." *Eng. Struct.*, 33(1), 53-62.

506

507 Valerio, P., and Ibell, T. J. (2003). "Shear strengthening of existing concrete bridges." *Struct.*
508 *Build.*, 156, 75-84.

509

510 Valerio, P., Ibell, T. J., and Darby, A. P. (2009). "Deep embedment of FRP for concrete shear
511 strengthening." *Struct. Build.*, 162, 311-321.

512

513 Xia, J., Jin, W. L., and Li, L. Y. (2011). "Shear performance of reinforced concrete beams
514 with corroded stirrups in chloride environment." *Corros. Sci.*, 53(5), 1794-1805.

515

516 Zakaria, M., Ueda, T., Wu, Z., and Meng, L. (2009). "Experimental investigation on shear
517 cracking behavior in reinforced concrete beams with shear reinforcement." *J. Adv. Concr.*
518 *Technol.*, 7(1), 79-96.

519

520

521

522

523

524

525

526

527

528

529

530

531

532

533

534

535

536

537

538

539

540

541 **LIST OF TABLES**

542 **Table 1 Test specimens**

543 **Table 2 Concrete properties**

544 **Table 3 Steel reinforcement properties**

545 **Table 4 Corrosion level results**

546 **Table 5 Test results**

547

548

549

550

551

552

553

554

555

556

557

558

559

560

561

562

563

564

565

566 Table 1 Test specimens

Group	Beam designation	Time of exposure to corrosion (sec)	Applied current density ($\mu\text{A}/\text{cm}^2$)	Targeted corrosion level (%)	Strengthening scheme
N	N00	-	-	-	All beams in Group N were unstrengthened
	N07	2006880	200	7	
	N12	4579200	185	15	
R	R00	-	-	-	10 mm CFRP rods @ 275 mm spacing
	R07	1995180	200	7	
	R12	6065940	140	15	
S	S00	-	-	-	One layer of continuous EB CFRP sheets
	S07	1998120	200	7	
	S12	4251600	200	15	

567

568

569

570

571

572

573

574

575

576

577

578

579

580

581

582

583

584

585 Table 2 Concrete properties

Beam designation	Cube compressive strength (MPa)		Cylinder split tensile strength (MPa)		Flexural strength (MPa)	
	Average ⁽¹⁾	Standard deviation ⁽¹⁾	Average ⁽²⁾	Standard deviation ⁽²⁾	Average ⁽²⁾	Standard deviation ⁽²⁾
N00	26.3	2.4	2.3	0.7	4.1	0.2
N07	35.1	1.0	2.6	0.2	5.4	0.4
N12	41.8	2.1	2.2	0.1	6.1	0.4
R00	21.7	1.3	1.5	0.2	3.1	0.2
R07	37.0	1.0	2.0	0.4	5.1	0.2
R12	37.0	1.3	1.9	0.1	5.3	0.4
S00	37.0	1.4	2.4	0	4.2	0.7
S07	36.8	0.9	2.5	0.3	5.4	0.5
S12	42.9	1.3	2.1	0.4	6.1	0.3

(1) Based on at least five samples per beam
(2) Based on three samples per beam

586
587
588
589
590
591
592
593
594
595
596
597
598
599
600
601
602

603 Table 3 Steel reinforcement properties

Bar diameter (mm)	Yield strength (MPa)	Yield strain (mm/mm)	Ultimate strength (MPa)	Elastic modulus (GPa)
8 (test span)	542	0.003	664	186
8 (non-test span)	573	0.003	655	183
20	576	0.003	707	179
25	537	0.003	669	180

604

605

606

607

608

609

610

611

612

613

614

615

616

617

618

619

620

621

622

623

624 Table 4 Corrosion level results

Shear link designation	Original mass (g)	Applied current (mA)	Applied current density ($\mu\text{A}/\text{cm}^2$)	Residual mass (g)	Theoretical corrosion level (%)	Actual corrosion level (%)	Average actual corrosion level (%)
N07/1 st	688	89.6	200	641	7.6	6.8	6.4
N07/2 nd	687	89.6	200	646	7.6	6.0	
N07/3 rd	683	89.2	200	640	7.6	6.3	
R07/1 st	684	89.4	200	634	7.5	7.3	7.6
R07/2 nd	693	90.5	200	642	7.5	7.4	
R07/3 rd	688	89.9	200	633	7.5	8.0	
S07/1 st	686	89.3	200	640	7.5	6.7	6.0
S07/2 nd	690	89.8	200	651	7.5	5.7	
S07/3 rd	691	90.0	200	652	7.5	5.6	
N12/1 st	690	83.3	185	609	16.0	11.7	12.2
N12/2 nd	689	83.3	185	611	16.0	11.3	
N12/3 rd	700	83.3	185	605	15.8	13.6	
R12/1 st	688	189*	140	612	15.9	11.0	12.3
R12/2 nd	699	189*	140	614	15.9	12.2	
R12/3 rd	692	189*	140	598	15.9	13.6	
S12/1 st	699	91.2	200	615	16.1	12.0	12.1
S12/2 nd	686	89.3	200	614	16.0	10.5	
S12/3 rd	687	89.5	200	592	16.0	13.8	

* Connected in series

625

626

627

628

629

630

631

632

633

634

635

636

637

638 Table 5 Test results

Beam designation	Average cube compressive strength (MPa)	Total shear force (kN)	Normalized shear stress at failure	Normalized shear stress at failure relative to N00	Deflection at loading point (mm)	Failure mode
N00	26.3	143	0.76	1.00	7.39	Shear
N07	35.1	148	0.68	0.89	8.73	Shear
N12	41.8	155	0.65	0.86	9.29	Shear
R00	21.7	142	0.83	1.09	9.57	Shear
R07	37.0	182	0.81	1.07	10.54	Shear
R12	37.0	164	0.73	0.96	9.69	Shear
S00	37.0	182	0.81	1.07	9.02	Shear
S07	36.8	174	0.78	1.03	7.62	Shear
S12	42.9	174	0.72	0.95	9.24	Shear

639

640

641

642

643

644

645

646

647

648

649

650

651

652

653

654

655

656 **LIST OF FIGURES**

657 **Figure 1 Cross-sections – all dimensions in mm**

658 **Figure 2 Test setup: (a) unstrengthened beams, (b) DE CFRP strengthened beams, and**
659 **(c) EB CFRP strengthened beams – all dimensions in mm**

660 **Figure 3 Accelerated corrosion setup**

661 **Figure 4 Shear force-deflection curves: (a) un-corroded beams, (b) 7% corroded beams,**
662 **(c) 12% corroded beams, and (d) EB strengthened beams**

663 **Figure 5 Unstrengthened beams at failure**

664 **Figure 6 Beams strengthened with the embedded CFRP rods at failure**

665 **Figure 7 Typical failure mode of the beams strengthened with the EB CFRP sheets**

666 **Figure 8 Shear force-strain curves: (a) outer shear links, (b) middle shear links, and (c)**
667 **inner shear links**

668 **Figure 9 Shear force-strain curves: (a) CFRP rods and (b) CFRP sheets**

669

670

671

672

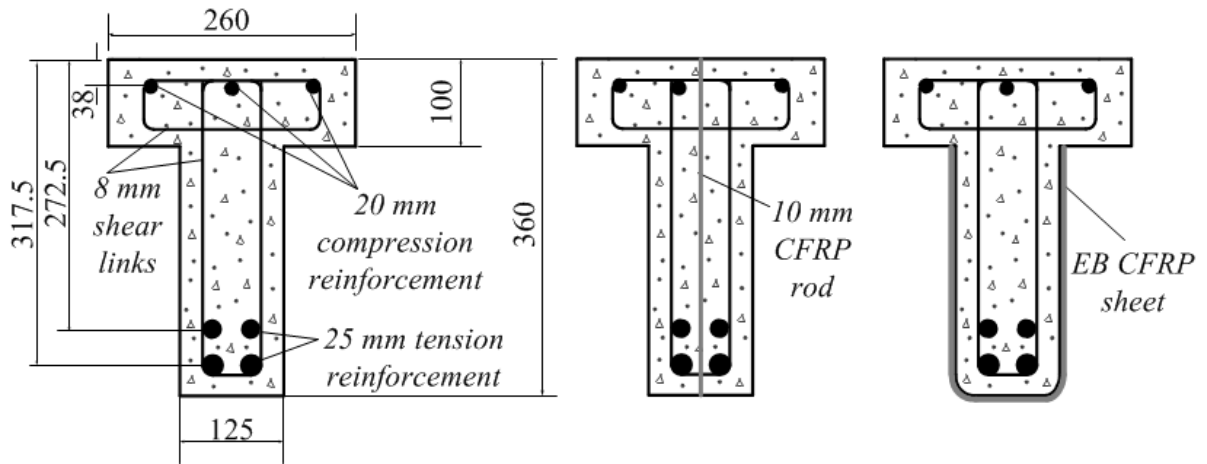
673

674

675

676

677



678

679

Figure 1 Cross-sections – all dimensions in mm

680

681

682

683

684

685

686

687

688

689

690

691

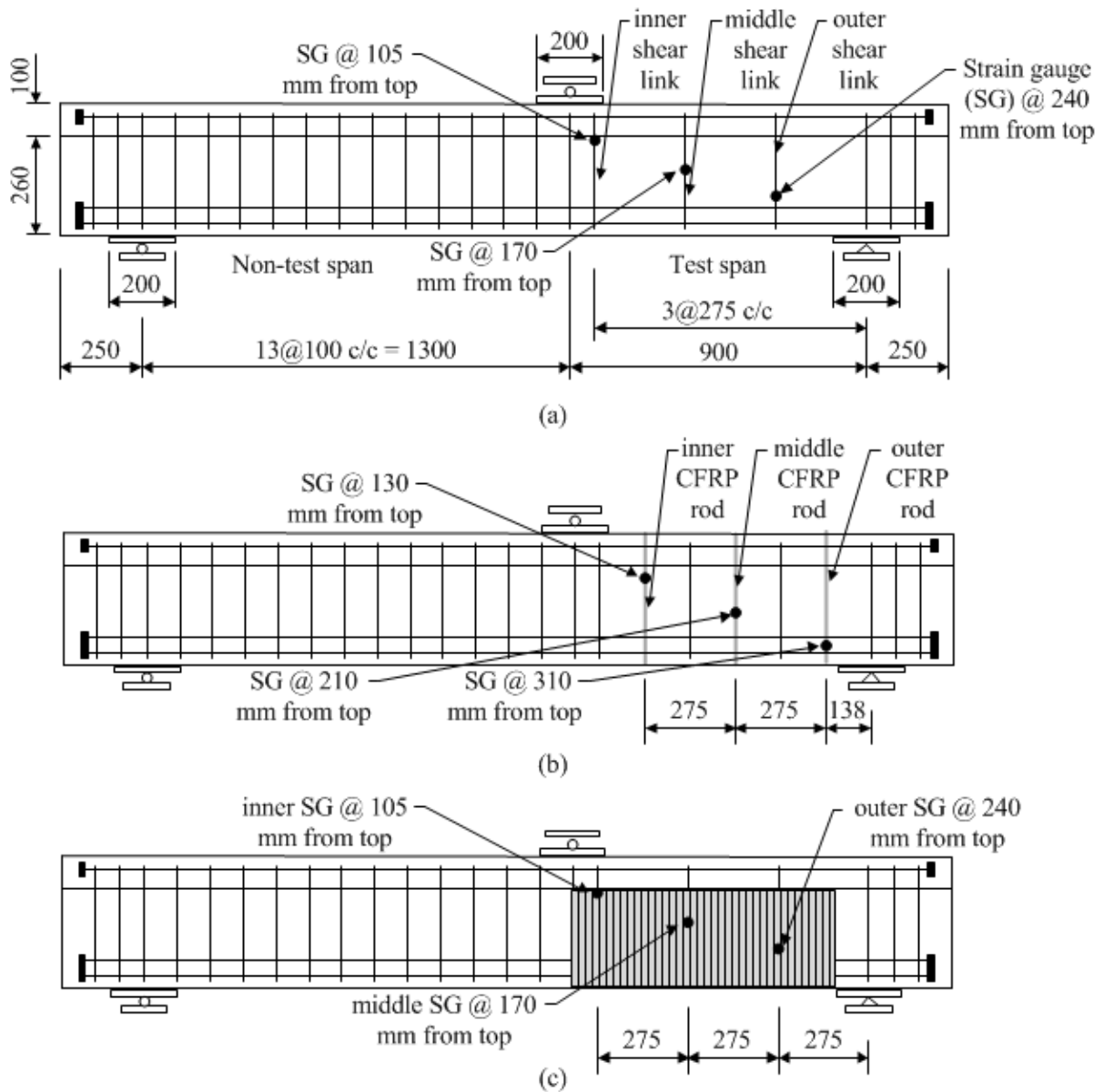
692

693

694

695

696



697

698 **Figure 2 Test setup: (a) unstrengthened beams, (b) DE CFRP strengthened beams, and**

699

(c) EB CFRP strengthened beams – all dimensions in mm

700

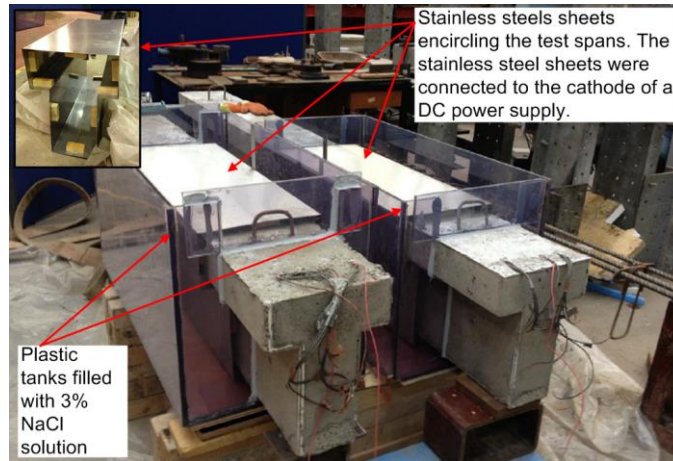
701

702

703

704

705



706

707

Figure 3 Accelerated corrosion setup

708

709

710

711

712

713

714

715

716

717

718

719

720

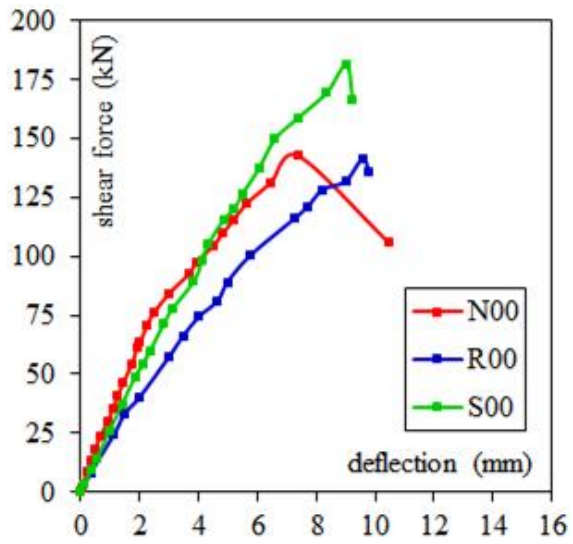
721

722

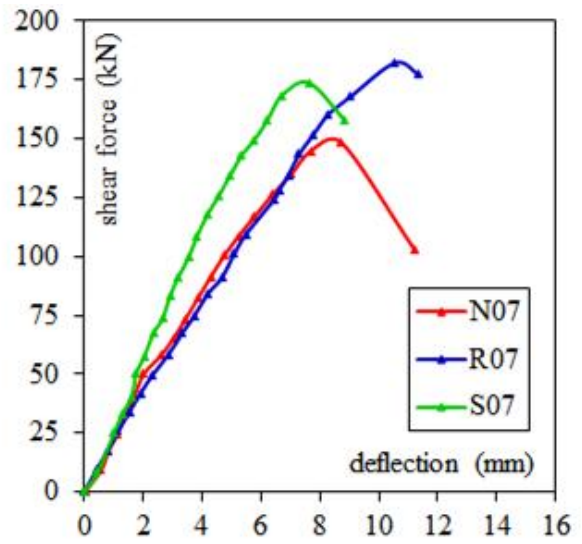
723

724

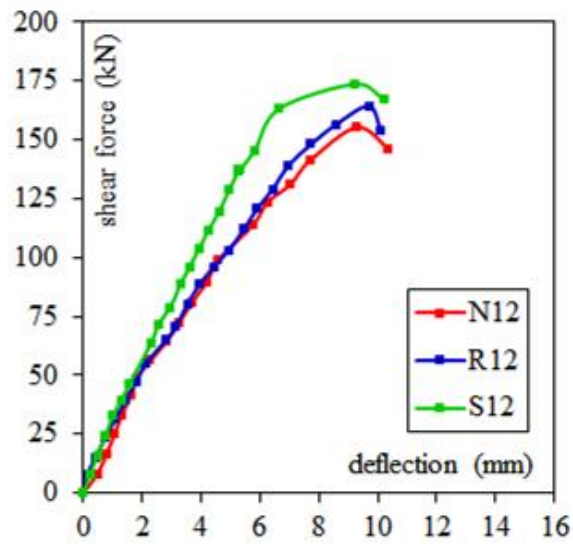
725



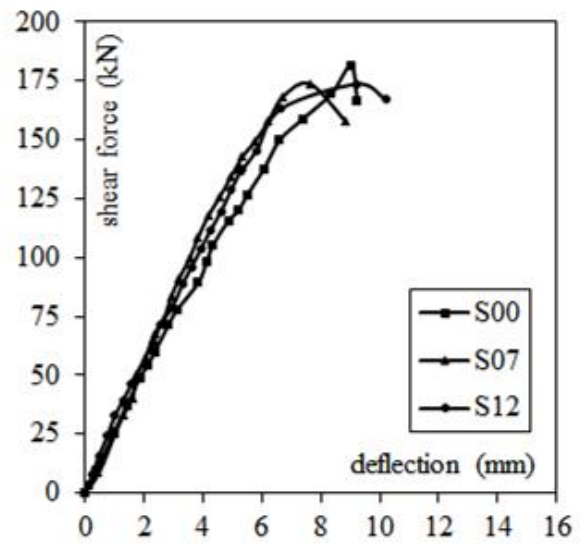
(a)



(b)



(c)



(d)

726

727 **Figure 4 Shear force-deflection curves: (a) un-corroded beams, (b) 7% corroded beams,**

728

(c) 12% corroded beams, and (d) EB strengthened beams

729

730

731

732

733

734

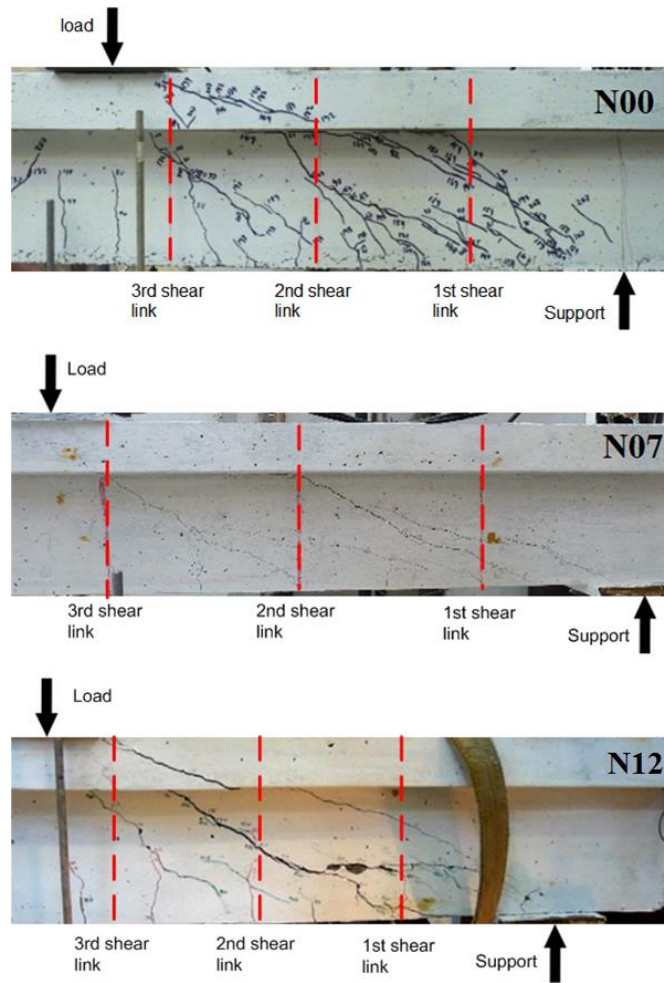


Figure 5 Unstrengthened beams at failure

735

736

737

738

739

740

741

742

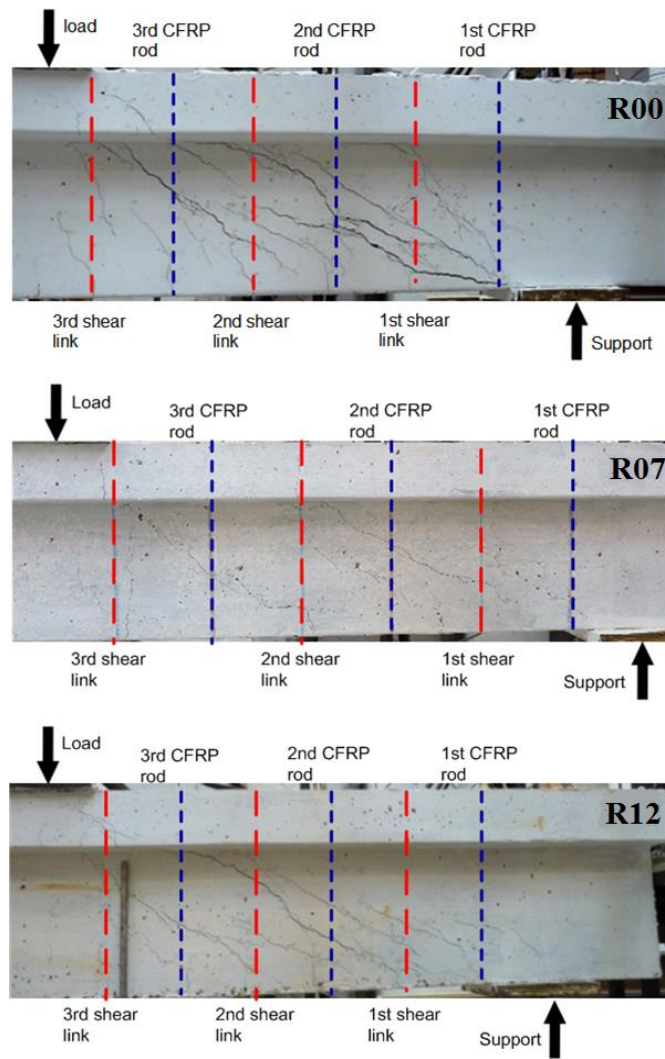
743

744

745

746

747



748

749

Figure 6 Beams strengthened with the embedded CFRP rods at failure

750

751

752

753

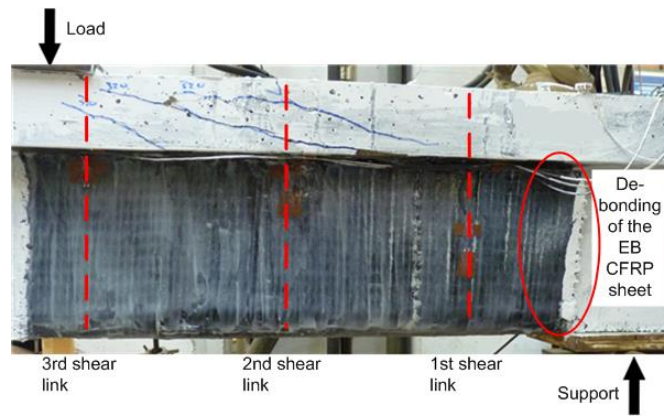
754

755

756

757

758



759

760

Figure 7 Typical failure mode of the beams strengthened with the EB CFRP sheets

761

762

763

764

765

766

767

768

769

770

771

772

773

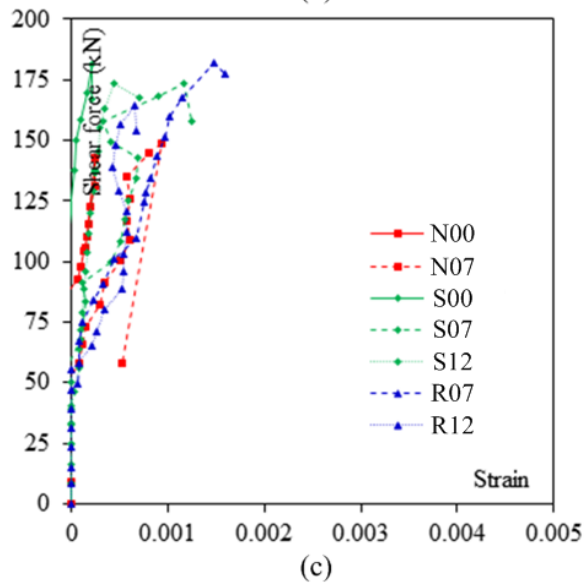
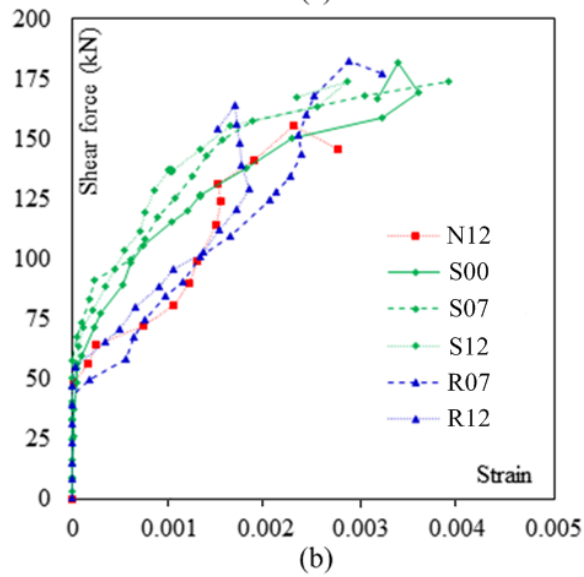
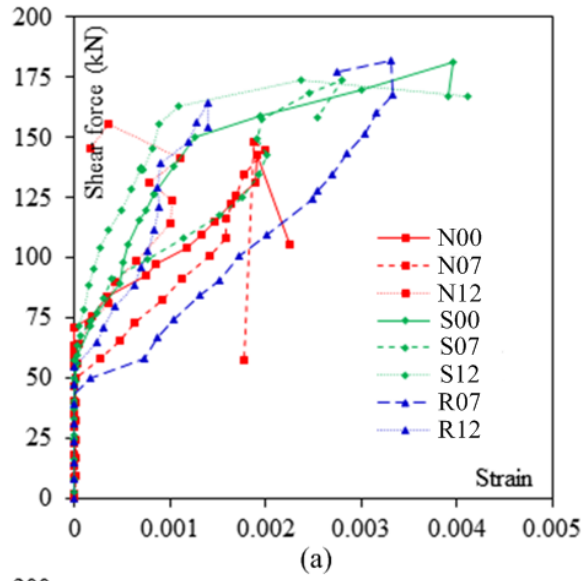
774

775

776

777

778



779

780

Figure 8 Shear force-strain curves: (a) outer shear links, (b) middle shear links, and (c)

781

inner shear links

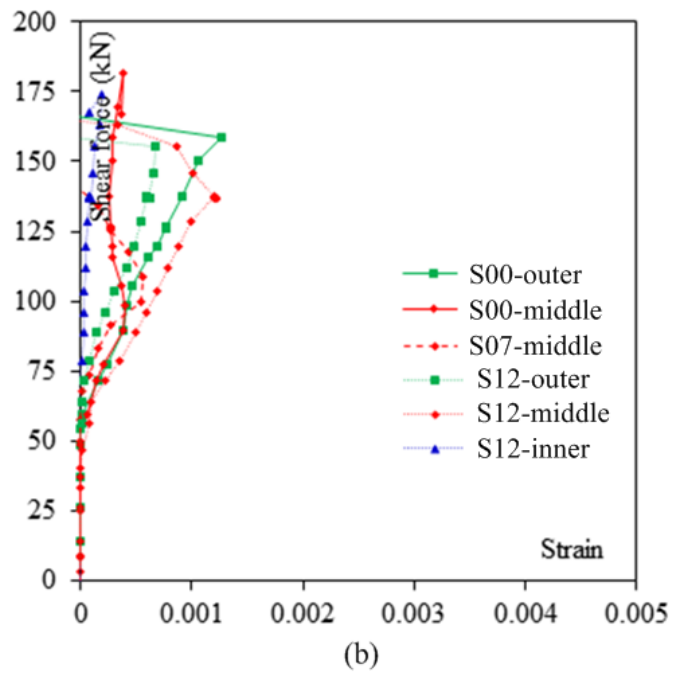
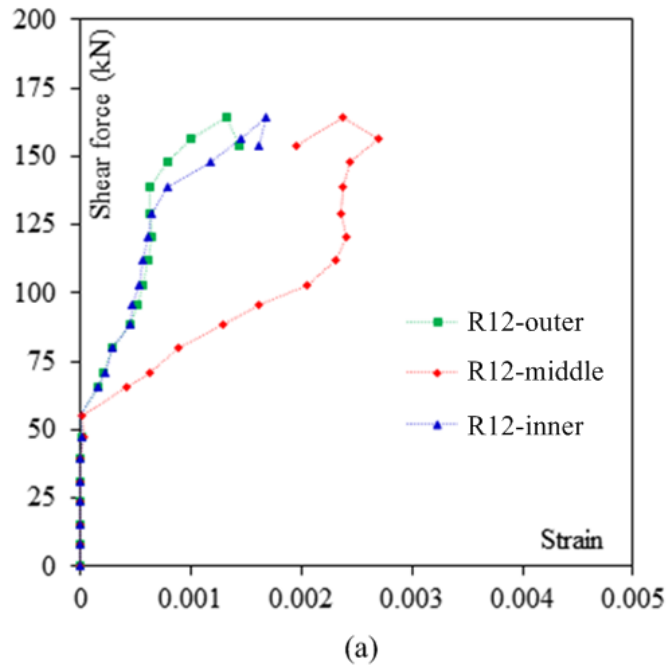


Figure 9 Shear force-strain curves: (a) CFRP rods and (b) CFRP sheets

782

783

784

785

786

787

788

789